Cellulose (2024) 31:4231–4245
https://doi.org/10.1007/s10570-024-05863-3

ORIGINAL RESEARCH

Distribution of carboxy groups in TEMPO-oxidized cellulose nanofibrils prepared from never-dried Japanese cedar holocellulose, Japanese cedar-callus, and bacterial cellulose

Yuko Ono · Yoshiki Horikawa · Miyuki Takeuchi · Ryo Funada · Akira Isogai

Received: 19 November 2023 / Accepted: 15 March 2024 / Published online: 21 March 2024
© The Author(s) 2024

Abstract We prepared 2,2,6,6-tetramethylpiperidine-1-oxyl (TEMPO)-oxidized samples from never-dried Japanese cedar (JC) holocellulose, JC-callus, and bacterial cellulose (BC). The original never-dried samples and their TEMPO-oxidized products were characterized by neutral sugar composition analysis. TEMPO-oxidized cellulose nanofibrils (TEMPO-CNFs) were prepared from the TEMPO-oxidized samples by ultrasonication in water. The carboxy groups in TEMPO-CNFs were position-selectively esterified with 9-anthryl diazomethane (ADAM) to prepare TEMPO-CNF-$COOCH_2$-$C_{14}H_9$ samples, which had UV absorption peak at 365 nm. The mass-average degree of polymerization (DP_w) values of 1% lithium chloride/*N*,*N*-dimethylacetamide (LiCl/DMAc) solutions of the original samples were determined by size-exclusion chromatography in combination with multi-angle laser-light scattering, ultraviolet absorption, and refractive index detection (SEC/MALLS/UV/RI), and were 5490, 2660, and 2380 for the JC holocellulose, JC-callus, and BC samples, respectively. The TEMPO-CNF-$COOCH_2$-$C_{14}H_9$ sample solutions in 1% LiCl/DMAc were analyzed by SEC/MALLS/UV/RI to obtain SEC elution patterns. The patterns corresponded to the molar mass and carboxy group distributions of the samples, which were detected by RI and UV absorption of anthryl groups, respectively. The carboxy groups existed in the entire molar mass distribution regions of all the TEMPO-CNF samples, although their lower molar mass regions contained higher carboxy group densities. The obtained results indicate that random depolymerization occurred on the cellulose microfibril surfaces at the initial stage of TEMPO-catalyzed oxidation and/or ultrasonication in water. This depolymerization mechanism can explain all the obtained SEC-elution patterns of the TEMPO-CNFs, without considering the presence of periodically disordered regions in the cellulose microfibrils of the never-dried cellulose samples.

Y. Ono · A. Isogai (✉)
Department of Biomaterials Science, Graduate School of Agricultural and Life Sciences, The University of Tokyo, Tokyo 113-8657, Japan
e-mail: akira-isogai@g.ecc.u-tokyo.ac.jp

Y. Horikawa · R. Funada
Institute of Agriculture, Tokyo University of Agriculture and Technology, Fuchu, Tokyo 183-8509, Japan

M. Takeuchi
Institute of Engineering Innovation, The University of Tokyo, Tokyo 113-8656, Japan

Graphical abstract

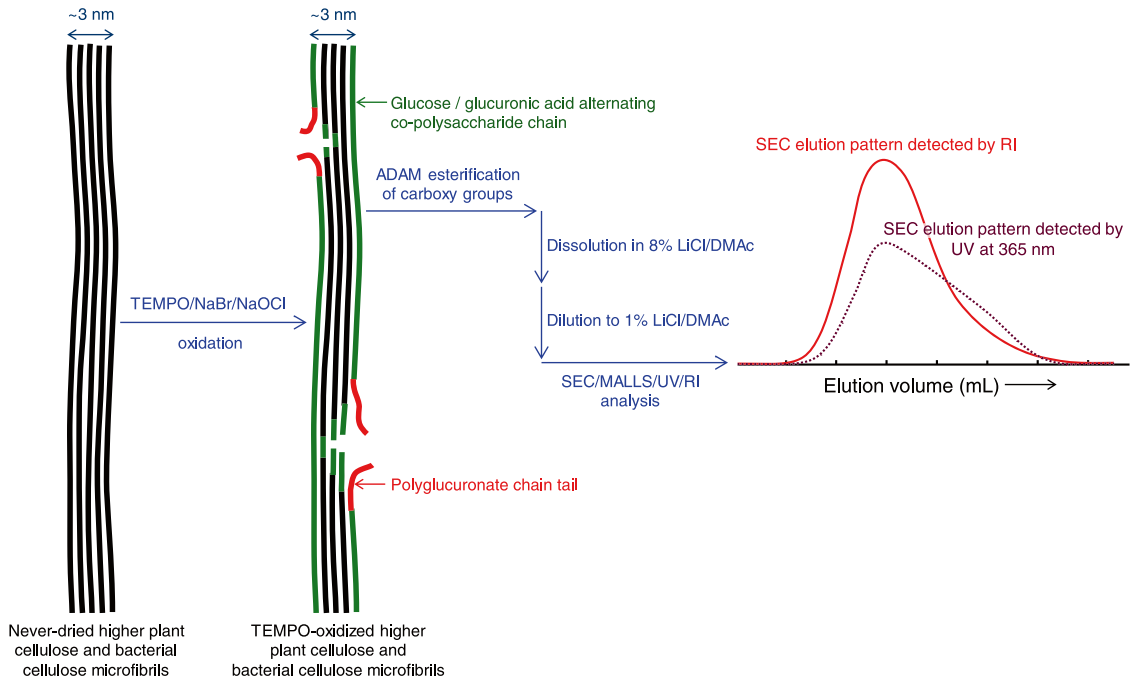

Keywords Cellulose microfibril · Distribution of carboxy group · Molar mass distribution · SEC/MALLS/UV/RI · TEMPO-CNF

Introduction

2,2,6,6-Tetramethylpiperidine-1-oxyl (TEMPO) is a stable water-soluble radical. When native cellulose samples are subjected to TEMPO-catalyzed oxidation in water at pH 10 and room temperature, numerous sodium C6-carboxy groups are formed on the cellulose microfibril surfaces (Isogai et al. 2018). Cellulose I crystal structures and crystallinities are mostly retained in TEMPO-oxidized products. TEMPO-oxidized cellulose samples with suitable carboxy group contents are convertible to gels consisting of individually nano-dispersed TEMPO-oxidized cellulose nanofibrils (TEMPO-CNFs) with similar widths by mechanical disintegration in water (Isogai et al. 2011; Isogai 2018). The widths of TEMPO-CNFs originate from those of the crystalline cellulose microfibrils present in the native cellulose samples (Okita et al. 2010). Therefore, TEMPO-catalyzed oxidation and subsequent mechanical disintegration in water to prepare TEMPO-CNFs can be used as a probe for structural analyses of native cellulose microfibrils, or for the investigation of individualized native cellulose microfibrils by transmission electron microscopy (TEM) or atomic force microscopy (AFM).

However, side reactions do occur. These include depolymerization (Zhou et al. 2020), the formation of C6-aldehyde groups (Shinoda et al. 2012) and sodium polyglucuronate homopolymer chains (Hirota et al. 2010), the additional oxidation of cellulose molecules inside each cellulose microfibril (Ono et al. 2021), and fibril shortening (Zhou et al. 2020) during TEMPO-catalyzed oxidation and subsequent mechanical disintegration in water. These side reactions depend on the oxidation and disintegration conditions (Hou et al. 2023). Therefore, it is important to carefully consider the side reactions described above during structural analyses of native cellulose microfibrils when TEMPO-catalyzed oxidation and subsequent mechanical disintegration in water is used as a probe. The TEMPO-CNFs investigated by TEM or AFM are, therefore, chemically treated cellulose nanofibrils containing numerous hydrophilic sodium

C6-carboxylate groups and other groups formed by side reactions, none of which exist in the original cellulose microfibrils.

Elucidating the distributions of carboxy groups in TEMPO-CNFs against their molar mass distributions may provide significant information about the packing structures of cellulose molecules and the distributions of periodically disordered structures in each crystalline native cellulose microfibril. Given that carboxy groups are formed on the crystalline cellulose microfibril surfaces and periodically disordered regions by TEMPO-catalyzed oxidation, and that partial depolymerization occurs preferentially at the periodically disordered regions, based on the core-clad structural model of native cellulose microfibrils (Hiraoki et al. 2014; Funahashi et al. 2017), the molar mass distributions of the TEMPO-CNFs should be somewhat bimodal. Furthermore, the carboxy groups should predominantly be present in lower molar mass regions formed by partial depolymerization during TEMPO-catalyzed oxidation.

In a previous paper, we position-selectively esterified the carboxy groups of algal cellulose, and those of commercial cotton lint and wood cellulose samples with 9-anthryl diazomethane (ADAM) to prepare TEMPO-CNF-$COOCH_2$-$C_{14}H_9$ samples. We investigated solutions of these samples in 1% (w/v) lithium chloride/*N*,*N*-dimethylacetamide (LiCl/DMAc) by size-exclusion chromatography in combination with multi-angle laser-light scattering, ultraviolet absorption, and refractive index detection (SEC/MALLS/UV/RI) (Ono et al. 2019). The SEC elution patterns of the algal cellulose detected by UV revealed that the carboxy groups existed in the low molar mass region. This was consistent with the structural model of TEMPO-oxidized cellulose microfibrils based on the core-clad model. However, the SEC-elution patterns for the cotton and wood cellulose samples indicated that the carboxy groups were distributed against the entire molar mass distributions, which is not consistent with periodically disordered cellulose microfibril structures. In the previous study, we used commercial cotton lint and wood cellulose samples, and their thermal or dying histories were, therefore, unknown.

In the present study, we prepared never-dried Japanese cedar (JC) holocellulose, purified JC-callus, and BC samples, and oxidized them in water at pH 10 using the TEMPO-catalysis system. The TEMPO-oxidized products were converted to TEMPO-CNFs by ultrasonication in water. The carboxy groups in the TEMPO-CNFs were esterified with ADAM. The distributions of anthryl groups in 1% LiCl/DMAc solutions of the TEMPO-CNF-$COOCH_2$-$C_{14}H_9$ samples were regarded as those of carboxy groups against the molar mass distributions, and were analyzed by SEC/MALLS/UV/RI. The packing models of the cellulose molecules in the microfibrils of each of the three samples were then determined from the SEC-elution patterns obtained by RI and UV.

Anthracene groups in the TEMPO-CNF-$COOCH_2$-$C_{14}H_9$ samples show fluorescence under laser-light irradiation depending on its wavelength. However, the laser light irradiation used in the present MALLS analysis had no influence on the scattered light pattern or UV absorption pattern at 365 nm in the entire SEC elution volume (Ono et al. 2019). The esterification of carboxy groups in cellulosic materials with 9H-fluoren-2-yl-diazomethane (FDAM) has already been reported for the distribution analysis of carboxy groups using a SEC/MALLS/RI system with a fluorescence detector (Bohrn et al. 2006; Henniges et al. 2006; Öztürk et al. 2008; Gehmayr et al. 2012; Milanovic et al. 2013; Zimmermann et al. 2016; Jusner et al. 2022). However, we used a commercial ADAM/hexane solution for esterification of the carboxy groups in TEMPO-CNFs because FDAM is not commercially available. Furthermore, UV detectors are attached to most of SEC/MALLS/RI systems in laboratories rather than fluorescence detectors.

Materials and methods

Samples

The Japanese cedar (*Cryptomeria japonica*) (JC) holocellulose was prepared from wood powder (particle size of ≥ 180 μm). The powder was dewaxed by soaking in 90% acetone/water and subsequent delignification with sodium chlorite ($NaClO_2$) in water at pH 4–5 and 70–80 °C for 1 h. This delignification was repeated six times (Ono et al. 2022a). JC callus tissue was obtained from young needles according to a previously published method (Yamagishi et al. 2015). Incubation was conducted on a solidified 0.2% gellan gum at 25 °C in the dark. The heterogeneously shaped JC-callus was converted to fine gel particles using a domestic blender. A JC-callus sample was

prepared by soaking the gel particles in 5% potassium hydroxide (KOH) for 1 d, then treating twice with $NaClO_2$ using the same procedure as described above (Hirano et al 2020). The KOH- and $NaClO_2$-treated JC-callus sample is hereafter referred to as JC-callus-2. The BC pellicles prepared by the cultivation of *Gluconacetobacter xylinus* (JCM10150) (Kim et al. 2002; Sun et al. 2017) were purified and converted to fine gel particles according to a previously reported method (Ono et al. 2022b). These JC holocellulose, JC-callus-2, and BC gel particles were stored in a never-dried state before use, and their solid contents in the wet state were measured from their dry mass contents obtained by heating potions of them at 105 °C for 3 h. ADAM and a 2 M trimethylsilyl diazomethane (TMSD) solution in diethyl ether were purchased from Sigma-Aldrich (USA) and Funakoshi Co., Ltd. (Tokyo, Japan), respectively. TEMPO, and other chemicals and solvents (FUJIFILM Wako Pure Chemicals, Tokyo, Japan) were of laboratory grade and used as received.

TEMPO-catalyzed oxidation of the never-dried samples

Based on the solid contents of the three wet samples, we prepared 1% (w/w, based on dry mass) sample suspensions in water. The TEMPO/sodium bromide (NaBr)/sodium hypochlorite (NaOCl) oxidation of the aqueous sample suspension was conducted at a constant pH of 10, and was controlled by the addition of 0.5 M NaOH. For the oxidation, we added 5 or 10 mmol/g NaOCl to the JC holocellulose, 5 mmol/g NaOCl to the JC-callus-2, and 5 or 10 mmol/g NaOCl to the BC sample, based on the dry mass of each sample (Shinoda et al. 2012). When no 0.5 M NaOH was consumed, $NaBH_4$ (~0.01 g) was added to the mixture at pH 10 in the same container, and the mixture was stirred for 3 h to reduce the low levels of C6-aldehydes present in the oxidized product to C6-OH groups (Takaichi et al. 2014). The mixture was then acidified to pH ~ 2.5 with dilute HCl to convert the COONa groups in the product to COOH groups. We obtained water-insoluble, TEMPO-oxidized products with protonated COOH groups by repeated washing with water through centrifugation, and stored them in the wet state before use. The solid contents of the wet TEMPO-oxidized products were measured by heating portions of them at 105 °C for 3 h. The mass recovery ratios of the TEMPO-oxidized products were calculated from the solid contents before and after oxidation.

Preparation of TEMPO-CNF/water dispersions

The wet TEMPO-oxidized JC and JC-callus-2 samples with protonated carboxy groups were suspended in water at a 0.1% solid content, and the TEMPO-oxidized BC samples were suspended at a 0.01% solid content. The COOH groups were converted to COONa groups by adding dilute NaOH to the suspension to form a solution with a pH of ~ 10. The TEMPO-oxidized JC holocellulose and BC samples were sonicated for 10 min, and the TEMPO-oxidized JC-callus-2 sample was sonicated for 6 min using an ultrasonic homogenizer (UTS300T, Nihon Seiki, Tokyo, Japan) at 300 W and 19.5 kHz power to prepare transparent TEMPO-CNF/water dispersions. Each dispersion was centrifuged at 12000 × *g* for 20 min, and the supernatants were collected as ~ 0.1% or ~ 0.01% TEMPO-CNF-COONa/water dispersions. The accurate solid content of each supernatant was determined by drying a portion of it at 105 °C for 3 h.

Esterification of the carboxy groups in the TEMPO-CNFs with TMSD or ADAM

A dilute HCl solution was added to the TEMPO-CNF-COONa/water dispersion containing ~ 100 mg (based on dry mass) of TEMPO-CNF-COONa to form a solution with a pH of ~ 2 for conversion to TEMPO-CNF-COOH. The TEMPO-CNF-COOH gel fraction of the acidic mixture was centrifuged and washed four times with methanol (40 mL each time) by centrifugation, during which almost all the TEMPO-CNF-COOH components were recovered as a methanol-insoluble fraction. After the final centrifugation to remove excess methanol, DMAc (30 mL) and methanol (6 mL) were added to the TEMPO-CNF-COOH. TMSD (0.5 mL containing 0.114 g or 1 mM TMSD) was added to the mixture, and it was stirred at room temperature for 1 h under a N_2 atmosphere for position-selective methyl esterification of carboxy groups in TEMPO-CNFs. Ethanol was added to the methyl-esterified product, and washed thoroughly three times with ethanol (40 mL each time) and finally with *t*-BuOH by centrifugation. The white powder product was obtained by freeze-drying

(Hiraoki et al. 2014; Tot et al. 2009; Ono et al. 2019, 2021). The methylation of the swollen gel samples suspended in the liquid TMSD/methanol/DMAc system proceeded heterogeneously (i.e., the TEMPO-CNFs were insoluble in the reaction medium before, during, and after methyl esterification).

In the case of esterification with ADAM, we prepared a solvent-exchanged TEMPO-CNF-COOH gel fraction (containing ~ 50 mg TEMPO-CNFs) from the TEMPO-CNF-COONa/water dispersion according to the same process described above. After centrifugation, DMAc (30 mL) and ADAM-containing DMAc (10 mL) were added to the sample containing a small amount of residual methanol. The sample was then stirred at 40 °C for 1 day in the dark under a N_2 atmosphere. The amount of ADAM dissolved in 10 mL DMAc was adjusted to 5 times the molar amount of carboxy groups in the TEMPO-CNFs. The 9-anthryl methyl-esterified TEMPO-CNFs in the mixture were isolated by washing thoroughly three times with ethanol (40 mL each time) and then with *t*-BuOH by repeated centrifugation, and successive freeze-drying (Ono et al. 2019). The esterification by ADAM of the swollen TEMPO-CNF gel particles suspended in the liquid ADAM/DMAc system proceeded heterogeneously (i.e., the TEMPO-CNFs were insoluble in the reaction medium before, during, and after esterification with ADAM).

Preparation of sample solutions in 1% LiCl/DMAc

The never-dried JC holocellulose, JC-callus-2, and BC samples were freeze-dried. The samples (8 or 16 mg each) were soaked in ethylenediamine (EDA). EDA was then exchanged for DMAc via methanol by repeated centrifugation without drying. After a final centrifugation to remove excess DMAc, 8% (w/w) LiCl/DMAc (2 mL) was added to each sample, which contained a small amount of residual DMAc. The resulting mixtures were stirred for up to 2 months to prepare transparent solutions, which were then diluted with fresh DMAc (14 mL) to form 0.05% or 0.1% sample solutions in 1% (w/v) LiCl/DMAc (Ono et al. 2016, 2022a, b, 2023). LiCl/DMAc solution (8% (w/w); 2 mL) was added to each freeze-dried methyl- and 9-anthryl methyl-esterified sample (8 or 16 mg), and the resulting mixtures were stirred for up to 1 week to obtain transparent solutions. Fresh DMAc (14 mL) was then added to each solution to prepare 0.05% or 0.1% sample solutions in 1% (w/v) LiCl/DMAc. Each sample solution in 1% (w/v) LiCl/DMAc was passed through a 0.45 μm disposable filter before SEC/MALLS/UV/RI analysis.

Analyses

Neutral sugar composition analysis of the original samples was performed according to a previously reported method (Ono et al. 2016; Hou et al. 2023): dissolution in 72% H_2SO_4, heating in 3% H_2SO_4 at 120 °C for 1 h, and high-performance liquid chromatography analysis of the hydrolysate (Hou et al. 2023). The carboxylate contents of the TEMPO-oxidized products were determined using an electrical conductivity titration method (Zhou et al. 2018; Hou et al. 2023). The SEC-elution patterns of the sample solutions, which were based on data determined by MALLS, IR, and UV absorption at 365 nm, were obtained using a SEC/MALLS/UV/RI system with 1% (w/v) LiCl/DMAc as an eluent (Hiraoki et al. 2014; Ono et al. 2016, 2019). Solid-state carbon 13 nuclear magnetic resonance (^{13}C-NMR) spectra were obtained according to a previously reported method (Zhou et al. 2020; Ono et al. 2019, 2022a; Hou et al. 2023). The particle size distributions of the TEMPO-CNF-COONa/water dispersions were determined over ~ 10 min using a particle size analyzer (Litesizer DLS 500, Anton Paar, Graze, Austria) equipped with a backside detection system to accumulate the data for each sample.

The detailed procedure for preparation of methyl- and 9-anthryl methyl-esterified TEMPO-CNFs prepared from never-dried JC and BC samples, and their SEC/MALLS/UV/RI analysis process are shown in Fig. 1.

Results

Preparation of TEMPO-oxidized products from wet samples

The JC holocellulose and JC-callus-2 samples were obtained in mass recovery ratios of 83% and 65%, based on the dry masses of the JC wood powder and JC-callus, respectively. The non-cellulosic compounds in these samples were partly removed during the repeated $NaClO_2$ treatment (and the 5% KOH

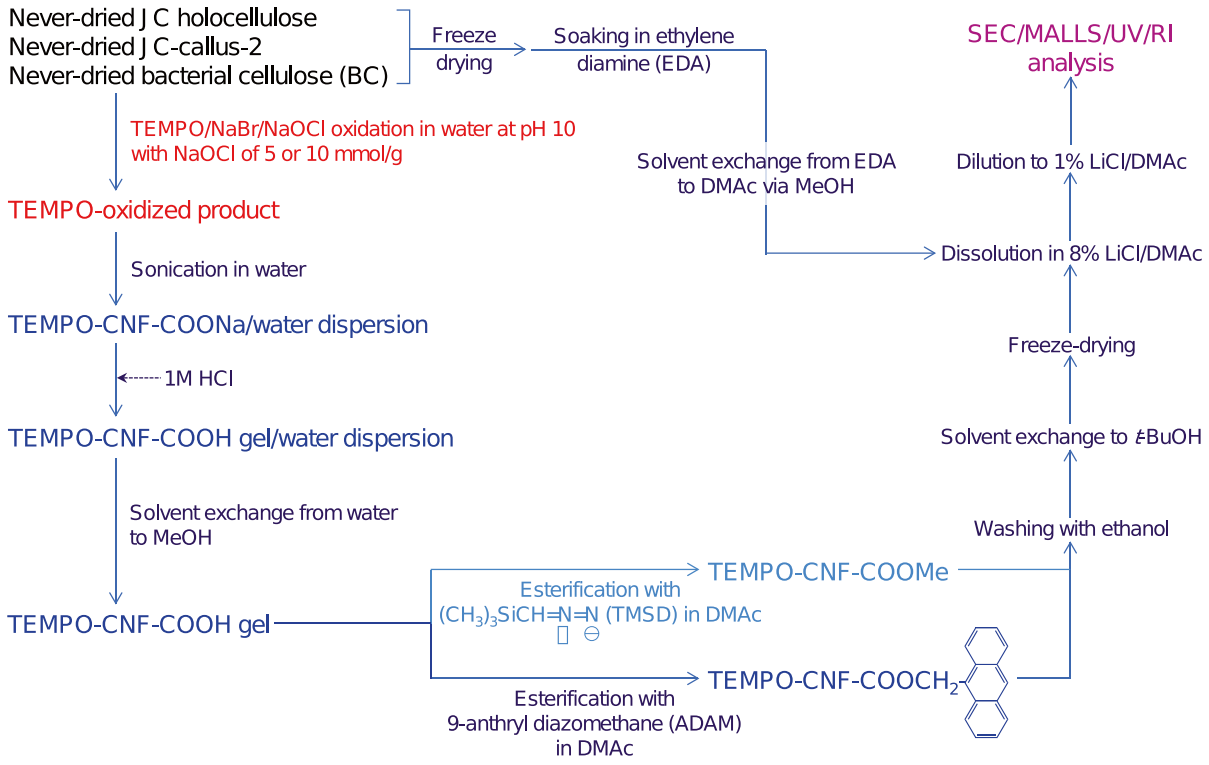

Fig. 1 Scheme for preparation of methyl- and 9-anthryl methyl-esterified TEMPO-CNFs prepared from never-dried JC and BC samples, and their SEC/MALLS/UV/RI analysis

treatment for the JC-callus), resulting in the mass recovery ratios given above. The mass recovery ratios of the TEMPO-oxidized JC holocellulose and JC-callus-2 products were 55% and 60%, respectively, based on the dry masses of the holocellulose samples. The hemicellulose in these samples was mostly removed as water-soluble fractions during washing by centrifugation, resulting in the mass recovery ratios given above. The TEMPO-oxidized BC products were obtained almost quantitatively from the original BC.

The results of neutral sugar composition analysis are listed in Table 1 with references. The "others" fractions comprised carboxy group-containing compounds originating from pectin, TEMPO-oxidized cellulose molecules, and $NaClO_2$-oxidized lignin. The hemicellulose-originating neutral sugars present in the JC holocellulose and JC-callus-2 samples were substantially removed by TEMPO-catalyzed oxidation. The JC-callus-2 had relatively large galactose, arabinose, and "others" contents, indicating that pectin remained in this sample, even after extraction with 5% KOH and subsequent $NaClO_2$ treatment. The pectin molecules present in the JC holocellulose and JC-callus-2 may have been mostly removed by TEMPO-catalyzed oxidation, because almost no galactose, arabinose, or rhamnose was present in the TEMPO-oxidized product. The levels of "others" fractions in the three samples were increased by oxidation because glucuronic acid units were formed from cellulose in the TEMPO-oxidized products.

The carboxy contents of the TEMPO-oxidized JC holocellulose and BC samples prepared with 5 mmol/g NaOCl were 1.0 and 1.1 mmol/g, respectively, and those prepared with 10 mmol/g NaOCl were 1.7 and 1.4 mmol/g, respectively. The carboxy contents of the TEMPO-oxidized JC-callus-2 could not be determined owing to an insufficient sample mass for the electrical conductivity titration. However, the C=O/C1 signal area ratio in the solid-state ^{13}C-NMR spectrum of this sample (Fig. 2, as described below) indicated a carboxy content of > 1.5 mmol/g, based on previously reported results (Ono et al. 2021, 2022b; Hou et al. 2023).

Table 1 Neutral sugar compositions (%, w/w) of the original JC, JC-callus, and BC samples, the JC and JC-callus-2 samples, and the TEMPO-oxidized products prepared with 5 mmol/g NaOCl

Sample	Glc	Gal	Man	Ara	Xyl	Rha	Others	Ref
JC	54.6	1.5	6.6	1.1	5.1	0.9	30.2	Ono et al. 2018
JC holocellulose	72.0	1.6	5.7	0.9	4.6	0.7	14.5	Ono et al. 2017
TEMPO-oxidized JC holocellulose	66.2	0.0	2.0	0.0	3.7	0.0	28.1	
JC-callus	26.2	4.2	1.4	6.9	5.6	2.1	53.6	
JC-callus-2	40.2	5.6	1.3	4.6	6.8	1.5	40.1	
TEMPO-oxidized JC-callus-2	40.6	0.0	0.8	0.0	2.5	0.0	56.0	
BC	90.6	0.0	+	+	+	0.0	9.4	Ono et al. 2022b
TEMPO-oxidized BC	59.9	0.0	+	+	0.0	0.0	40.1	Ono et al. 2022b

JC Japanese cedar, *BC* bacterial cellulose, *TEMPO* 2,2,6,6-tetramethylpiperidine-1-oxyl radical

The solid-state ^{13}C-NMR spectra of the JC-callus-2 and its TEMPO-oxidized product are shown in Fig. 2. The JC-callus-2 produced an intense carboxy carbon signal, indicating the presence of pectin. After TEMPO-catalyzed oxidation, the carboxy carbon and amorphous C4 carbon peak areas centered at 175 and 84 ppm, respectively, decreased. This indicated that the amorphous pectin molecules containing carboxy groups present in the JC-callus-2 had been removed from the water-insoluble TEMPO-oxidized product as water-soluble oxidized and degraded compounds. The carboxy carbon peak at 174 ppm present in the TEMPO-oxidized product can probably be attributed to the C6-OH groups formed on the crystalline cellulose microfibril surfaces by TEMPO-catalyzed oxidation.

TEMPO-CNF/water dispersions

Transparent TEMPO-CNF/water dispersions were obtained from the TEMPO-oxidized JC holocellulose, JC-callus-2, and BC samples by ultrasonication in water and subsequent centrifugation to remove fine metal particles formed from the tip of the ultrasonic homogenizer. The mass recovery ratios of the TEMPO-CNFs based on their TEMPO-oxidized samples were almost 100%; there were almost no unfibrillated fractions in any of the dispersions obtained by ultrasonication. The particle size distributions of the TEMPO-CNFs in the dispersions at various TEMPO-CNF contents were determined for the TEMPO-oxidized JC holocellulose and JC-callus-2 samples, and the results are shown in Fig. 3. Each TEMPO-CNF dispersion had a suitable TEMPO-CNF content, as shown in the green range in Fig. 3a, so that reliable and reproducible average particle sizes could be obtained (Fig. 3a). When the TEMPO-CNF content was higher than the suitable content, the TEMPO-CNFs formed network structures in the dispersion, resulting in a larger average particle size. When the TEMPO-CNF content was significantly lower than the suitable content, the scattered light intensity became low, resulting in inaccurate average particle sizes.

Solid-state ^{13}C-NMR spectra of JC holocellulose-related materials

The solid-state ^{13}C-NMR spectra of the JC holocellulose and TEMPO-oxidized JC holocellulose, and the methyl- and 9-anthryl methyl-esterified samples preferred from the TEMPO-CNFs are shown in Fig. 4. The broad signals at 110–156 ppm are ascribed to aromatic carbons of residual lignin in the JC holocellulose (Ono et al. 2022a). The methoxy methyl carbon peak of the residual lignin was also detected at 56 ppm. The broad carboxy signal at 160–180 ppm was formed by oxidative degradation of aromatic rings of lignin in $NaClO_2$-oxidation (Ono et al. 2022a). The aromatic and methoxy carbon signals originating from the residual lignin disappeared by TEMPO-catalyzed oxidation, showing that the residual lignin components were mostly removed as water-soluble and degraded compounds from the water-insoluble TEMPO-oxidized JC holocellulose. The carboxy carbon peak at 174 ppm is primarily formed from the C6-OH groups present on the crystalline cellulose microfibril surfaces and facing the outside in the JC holocellulose by TEMPO-catalyzed oxidation.

The amorphous C4 peak at 84 ppm increased in intensity during the ultrasonication of the TEMPO-oxidized

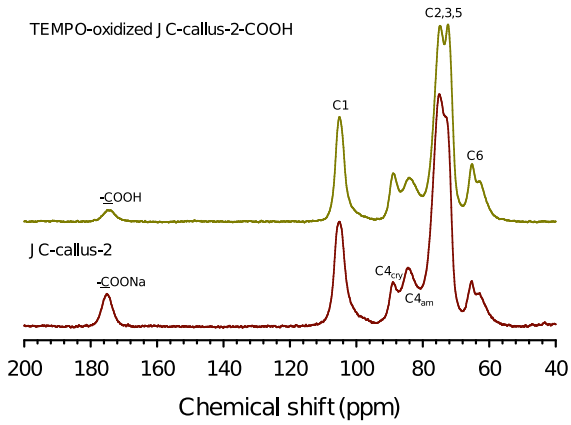

Fig. 2 Solid-state ^{13}C-NMR spectra of JC-callus-2 and its TEMPO-oxidized product

product in water and the subsequent methyl esterification of the carboxy groups (Zhou et al. 2020). A peak attributable to methyl-esterified carboxy carbons was located at 172 ppm, and a peak attributable to methyl carbons appeared at 55 ppm. The carboxy carbon peak shifted to 170 ppm during esterification with ADAM, and the aromatic carbon signals produced by the anthryl groups appeared at 120–136 ppm. Although the solid-state ^{13}C-NMR analysis was not conducted in the quantitative mode, the aromatic carbon/C1 and methyl carbon/C1 signal area ratios indicated that the carboxy groups in the TEMPO-oxidized JC holocellulose were mostly esterified with TMSD and ADAM, respectively, by the esterification procedures described in the Experimental section. Therefore, it was possible to use the anthryl groups as markers of carboxy groups in the TEMPO-CNFs. Furthermore, the SEC-elution patterns detected for the ADAM-treated TEMPO-CNFs by UV absorption can be regarded as indicating the corresponding distributions of carboxy groups in the TEMPO-CNFs in the following section.

SEC/MALLS/UV/RI analysis of the JC holocellulose, JC-callus-2 and BC samples, and their esterified products

Figure 1 in Experimental section is a scheme showing SEC/MALLS/UV/RI analysis of the JC holocellulose, JC-callus-2, and BC samples, and their TEMPO-CNFs after esterification of the carboxy groups with TMSD or ADAM. The molar mass parameters of the JC holocellulose, JC-callus-2, and BC samples before TEMPO oxidation were obtained by soaking the freeze-dried samples in EDA and subsequently exchanging EDA for DMAc via methanol. All the samples were analyzed using 1% (w/v) LiCl/DMAc as the eluent, and the same SEC column and system. This is advantageous for comparisons of the SEC elution patterns produced by the original samples and their TEMPO-CNFs.

The SEC-elution patterns of JC holocellulose and its TEMPO-CNFs prepared with 5 or 10 mmol/g NaOCl were obtained by measuring the RI values and the UV absorption at 365 nm, and are shown

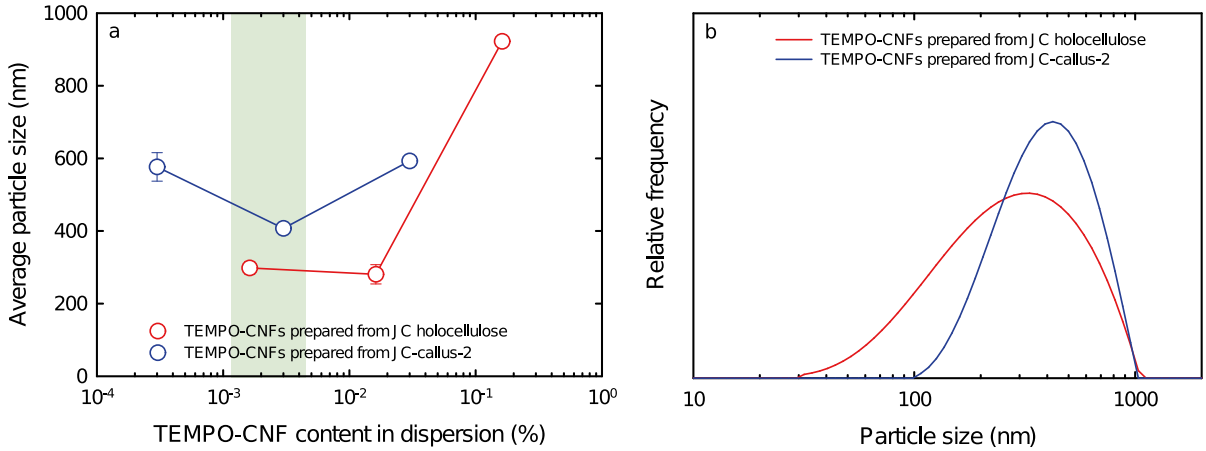

Fig. 3 **a** Relationships between TEMPO-CNF content in the dispersions and the average particle size of the TEMPO-CNFs prepared from JC holocellulose and JC-callus-2, and (**b**) particle size distributions of the two TEMPO-CNFs prepared with 5 mmol/g NaOCl

in Fig. 5. The SEC-elution patterns of the TEMPO-CNFs obtained by measuring the RI shifted to a higher elution volume (or a smaller molar size) from that of the original JC holocellulose, indicating partial depolymerization during TEMPO-catalyzed oxidation and subsequent ultrasonication in water to prepare the TEMPO-CNFs. The DP_w value of the JC holocellulose determined by SEC/MALLS/RI was 5490, which decreased to 1490 following TEMPO-catalyzed oxidation with 5 mmol/g NaOCl and subsequent ultrasonication in water. Herein, the DP_w value of the TEMPO-CNFs prepared from the JC-holocellulose was determined from the SEC/MALLS/RI data for the TEMPO-CNF-$COOCH_3$ (Hiraoki et al. 2014; Ono et al. 2019).

The ADAM-esterified TEMPO-CNFs prepared from the JC holocellulose exhibited clear UV absorption in the entire molar mass regions. In contrast, the methyl-esterified TEMPO-CNFs absorbed almost no UV. When the SEC-elution patterns of the TEMPO-CNF-$COOCH_2$-$C_{14}H_9$ samples obtained by RI detection were compared with those obtained by UV absorption, the carboxy groups were present in the entire molar mass distribution regions. However, the carboxy groups were distributed in higher densities in the lower molar mass regions.

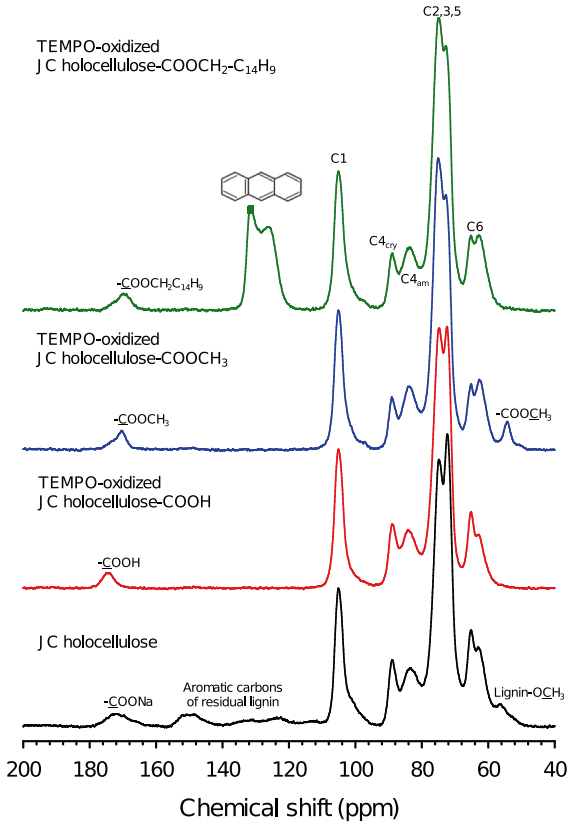

Fig. 4 Solid-state ^{13}C-NMR spectra of JC holocellulose, TEMPO-oxidized JC holocellulose, and the methyl- and 9-anthryl methyl-esterified products prepared from the TEMPO-CNFs

Similar results to those in Fig. 5 were obtained for the TEMPO-CNFs prepared from the JC-callus-2 (Fig. 6). The small peak in the elution volume of the JC-callus-2 at ~ 9 mL is probably attributable to non-cellulosic compounds (such as hemicelluloses and pectin) present in the sample, and almost disappeared following TEMPO-catalyzed oxidation and subsequent ultrasonication in water. The DP_w of the original JC-callus-2 was 2660. The DP_w of the TEMPO-oxidized and subsequently ultrasonicated product could not be determined because the sample amount was insufficient for additional methyl esterification experiment. However, the SEC-elution pattern of TEMPO-CNF-$COOCH_2$-$C_{14}H_9$ determined by RI detection indicated a DP_w value of > 1500, based on the results presented in Fig. 5. The anthryl groups detected by UV absorption at 365 nm as markers of carboxy groups in the TEMPO-CNFs were present in the entire molar mass region of the product, although the carboxy group density was higher in the lower molar mass region.

The SEC-elution patterns of the BC, TEMPO-CNF-$COOCH_3$, and TEMPO-CNF-$COOCH_2$-$C_{14}H_9$ samples prepared from BC with 5 or 10 mmol/g NaOCl, and detected by RI and UV absorption at 365 nm, are shown in Fig. 7. The results were similar to those presented in Figs. 5 and 6: 1) depolymerization occurred on the TEMPO-CNFs, and the DP_w decreased from 2380 for the original BC to 1530 and 1120 for the TEMPO-CNFs prepared with 5 and 10 mmol/g, respectively, followed by ultrasonication in water; 2) the methyl-esterified products did not absorb UV; 3) the SEC elution patterns of the methyl-esterified products detected by RI were similar to those of the 9-anthryl methyl-esterified products determined in the same way; and 4) the carboxy groups were present in the entire molar mass regions, but were present in higher densities in the lower molar mass regions.

Figure 8 shows the relative value of the UV absorption to RI intensity (UV/RI) at each SEC elution volume for the five samples shown in Figs. 5, 6, and 7, showing the concentration of anthracene-methyl

ester groups per mass at each SEC elution volume. Although the concentrations of anthracene-methyl groups in the low-molar-mass regions were higher than those in the high-molar-mass regions, the five samples had significantly high concentrations of anthracene-methyl groups in the high molar-mass-regions. Thus, the C6-carboxy groups in the TEMPO-CNFs prepared from the never-dried JC holocellulose, JC-callus, and BC were more distributed throughout the molecules ranging from low to high molar masses.

Discussion

The structures of the cellulose microfibrils in the native cellulose of higher plants and BC have not been definitively determined. Leveling-off average DPs (LODPs) of 200–300 determined for commercial higher plant cellulose samples, such as chemical wood pulps, cotton lint, and linters cellulose, by dilute acid hydrolysis indicate the presence of periodically disordered regions along the longitudinal directions of native cellulose microfibrils (Borrega et al. 2018; Horikawa et al. 2018; Funahashi et al. 2018). Neutron-scattering analysis of commercial ramie cellulose fibers also indicates the presence of periodically disordered regions (Nishiyama et al. 2003).

LODP values have been obtained from never-dried higher plant cellulose samples that had been subjected to hydrolysis by dilute acid, but they were higher than those obtained from dried samples (Funahashi et al. 2018). Therefore, it has been hypothesized that the disordered regions indicated by LODPs in higher plant cellulose samples are artificially formed during drying or other processes (Einfeldt et al. 2005; Håkansson and Ahlgren 2005; Atalla et al. 2014; Funahashi et al. 2018). Furthermore, SEC/MALLS/RI analysis of microcrystalline cellulose samples produced from cotton linters cellulose, and pulps by hydrolysis with dilute acid indicates wide DP ranges of 60–600 (although their average DP values are always 200–300) (Funahashi et al. 2018; Ono et al. 2018; Ono and Isogai 2021). It is not plausible that such wide DP values, which correspond to the lengths of crystalline regions, are controlled by biosynthetic processes and are formed in pristine and never-dried plants.

If the core-clad structures of cellulose molecules with periodically disordered regions are assumed to be present in each higher plant cellulose microfibril, the SEC elution patterns of TEMPO-CNFs with sufficiently high DPs detected by RI and UV absorption at 365 nm should exhibit the patterns shown in Fig. 9. The core cellulose molecules in each microfibril should exhibit higher molar masses with lower carboxy densities. However, the surface cellulose molecules had lower molar masses with higher carboxy densities. The formation of alternating glucose/glucuronic acid co-polymers with polyglucuronic acid homopolymer chains has been demonstrated in TEMPO-CNFs prepared from wood and tunicate

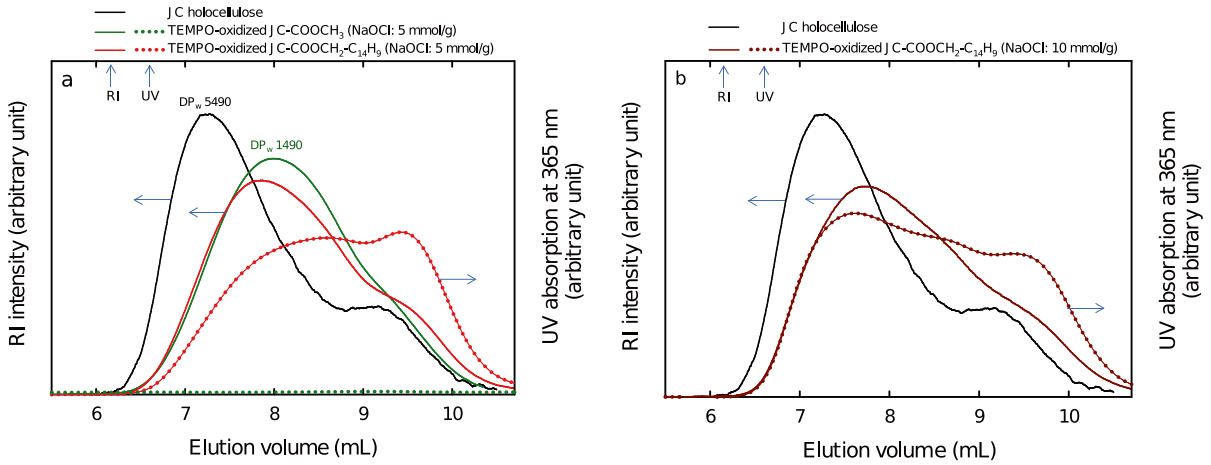

Fig. 5 SEC-elution patterns of original JC holocellulose and TEMPO-oxidized JC holocellulose products prepared with (**a**) 5 mmol/g NaOCl and (**b**) 10 mmol/g NaOCl, obtained by RI detection and UV absorption at 365 nm

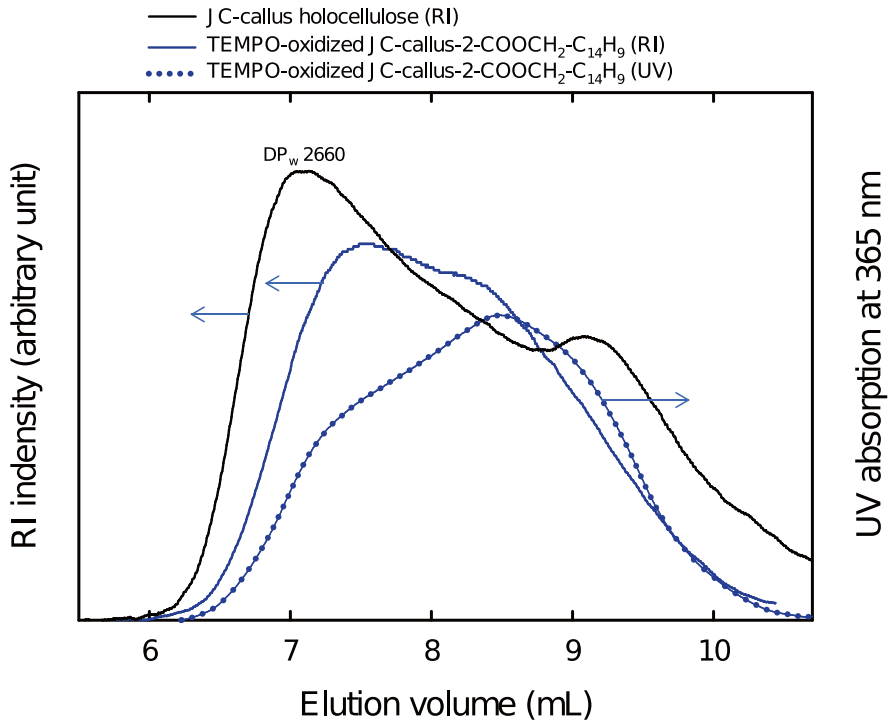

Fig. 6 SEC-elution patterns of the original JC-callus-2 and TEMPO-oxidized JC-callus-2 prepared with 5 mmol/g NaOCl, obtained by RI detection and UV absorption at 365 nm

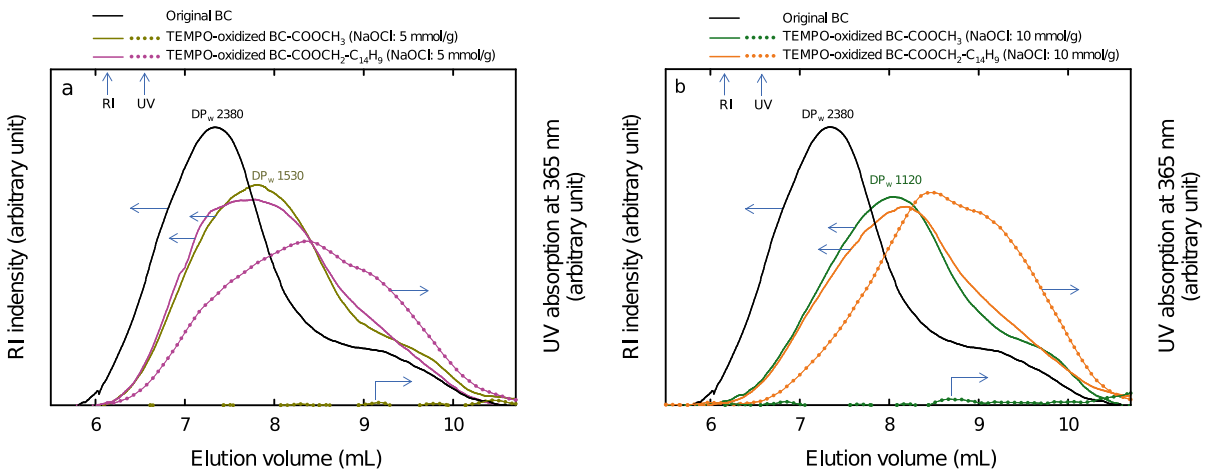

Fig. 7 SEC-elution patterns of the original BC and TEMPO-oxidized BC products prepared with (**a**) 5 mmol/g NaOCl and (**b**) 10 mmol/g NaOCl, obtained by RI detection and UV absorption at 365 nm

cellulose samples by surface peeling with 10% NaOH (Hirota et al. 2010).

The carboxy groups formed by TEMPO-catalyzed oxidation were widely distributed to the entire molar mass distribution ranges of TEMPO-CNFs when never-dried JC holocellulose, JC-callus-2, and BC samples were used in the present study, as shown in Figs. 5, 6, and 7. Consequently, irrespective of whether commercial higher plant cellulose, never-dried higher plant cellulose, or BC samples, the cellulose microfibril model shown in Fig. 10 can explain the obtained results without inconsistencies. In TEMPO-CNFs with DP_w values of > 1000, the initial depolymerization points are randomly

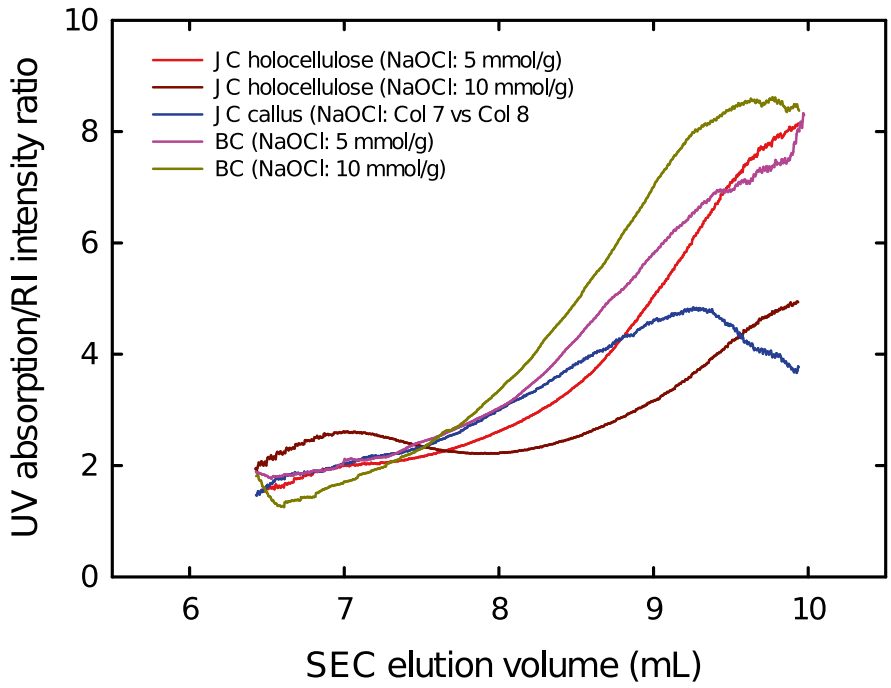

Fig. 8 Relationship between SEC elution volume and the UV absorption/RI intensity ratios for the five anthracene-methyl-esterified TEMPO-CNFs in Figs. 5, 6, and 7

formed on the cellulose microfibril surfaces. Oxidation and depolymerization may proceed to cellulose molecules inside the microfibril from the initially depolymerized point, but will not proceed to the surrounding surface chains as in the model shown in Fig. 9.

The model shown in Fig. 10 can also explain the SEC-elution patterns for fibrous TEMPO-oxidized

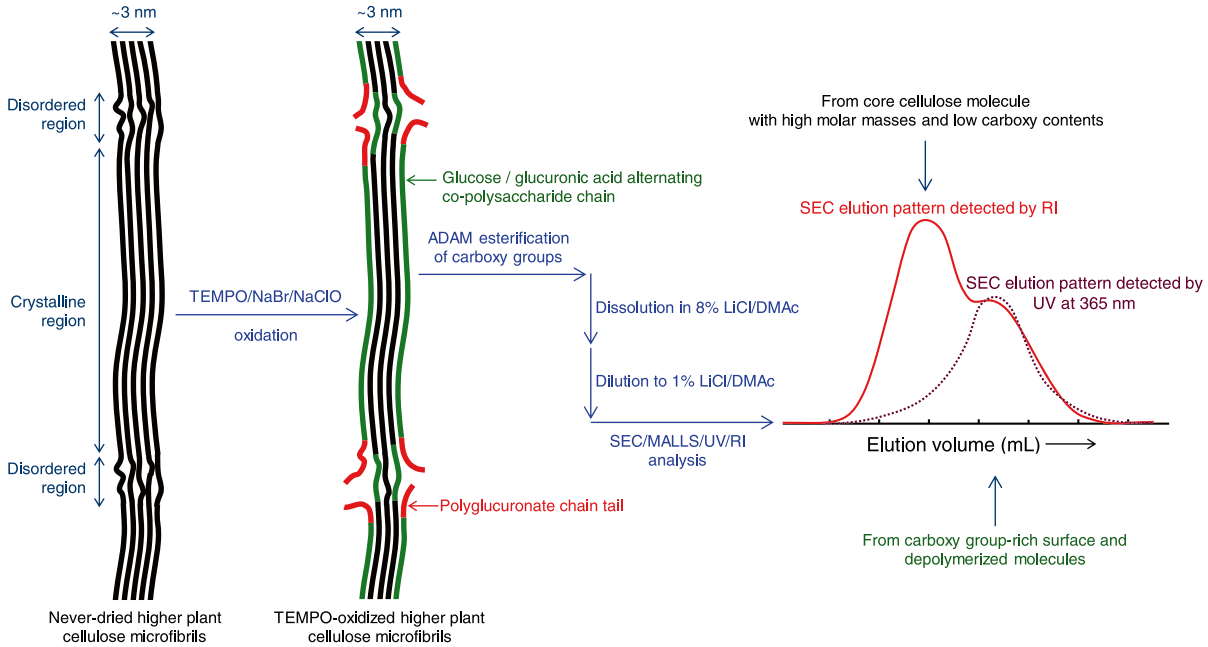

Fig. 9 A hypothetical model of cellulose microfibrils containing disordered regions periodically distributed along the longitudinal direction, and the resultant hypothetical carboxy group distribution pattern against the molar mass distribution of the TEMPO-CNFs

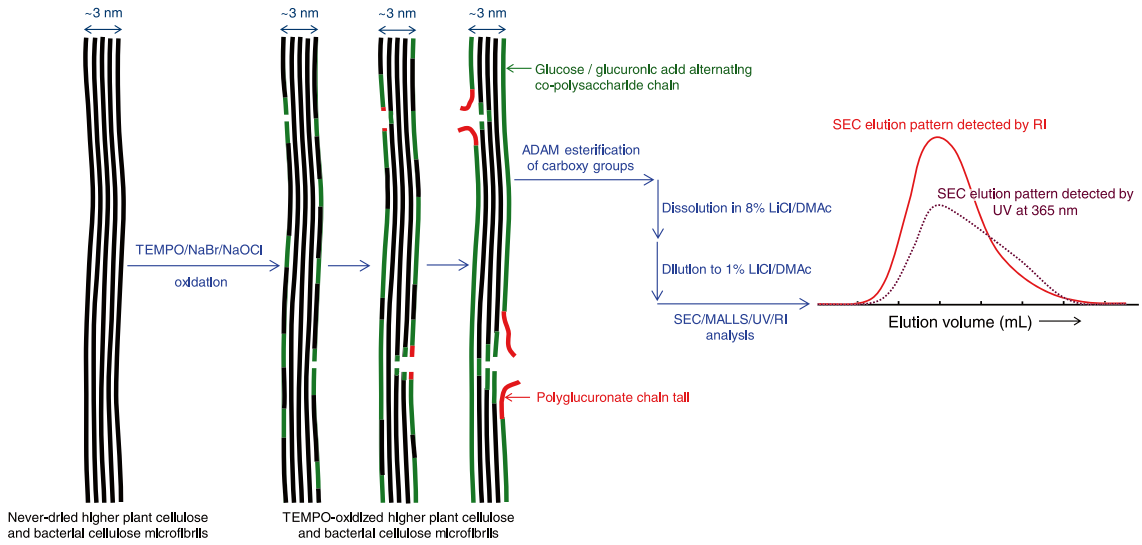

Fig. 10 A possible model of cellulose microfibrils without considering the presence of periodically disordered regions, and the resultant hypothetical carboxy group distribution pattern against molar mass distribution in SEC-elution patterns of TEMPO-CNFs

pulps before ultrasonication in water and also for TEMPO-CNFs obtained after ultrasonication in water, when detected by RI (Hiraoki et al. 2014; Zhou et al. 2020; Ono et al. 2022b). The SEC elution patterns of TEMPO-oxidized pulps and TEMPO-CNFs had mostly single peaks (without clear bimodal peaks, as in the model shown in Fig. 10). The SEC peak position gradually shifted to a lower molar mass (or higher elution volume) as the amount of NaOCl (the primary oxidant in TEMPO-catalyzed oxidation) increased, or the ultrasonication time of the fibrous TEMPO-oxidized samples in water increased. Therefore, during TEMPO-catalyzed oxidation, periodically disordered regions are not detectable by chemical species responsible for depolymerization, even if they are present in never-dried native cellulose samples. This is probably because the active chemical species that cause depolymerization in TEMPO-catalyzed oxidation are much larger than the H^+ in dilute acid hydrolysis. Consequently, depolymerization occurs randomly on cellulose microfibril surfaces during TEMPO-catalyzed oxidation.

Conclusions

TEMPO-CNFs prepared from never-dried JC holocellulose, JC-callus-2, and BC samples by TEMPO-catalyzed oxidation and subsequent ultrasonication in water had DP_w values of > 1000. The carboxy groups in the TEMPO-CNFs were position-selectively 9-anthryl methyl-esterified without drying from the never-dried state. Here, a commercially available ADAM/hexane solution was successfully used for the position-selective esterification. We prepared 1% (w/v) LiCl/DMAc solutions of TEMPO-CNF-$COOCH_2$-$C_{14}H_9$ and TEMPO-CNF-$COOCH_3$ samples, and subjected them to SEC/MALLS/UV/RI analysis. SEC elution patterns provided molar mass distributions detected by RI and carboxy group distributions detected by UV absorption at 365 nm. Carboxy groups were present in the entire molar mass distribution regions in all the TEMPO-CNF samples, although their lower molar mass regions contained higher carboxy group densities (Fig. 8). The periodically disordered structure model used to explain the LODPs of higher plant cellulose samples that have undergone hydrolysis with dilute acid was investigated to explain the results obtained herein. However, without considering the periodically disordered regions, the random depolymerization on the cellulose microfibril surfaces during the initial stage of TEMPO-catalyzed oxidation and/or ultrasonication in water can explain the results obtained in the present study without inconsistency.

Acknowledgments We thank Edanz for editing a draft of this manuscript.

Author contributions YO and AI proposed the concept. YO mainly conducted the experiments. All of the authors contributed to the analyses. All of the authors read and approved the final manuscript. The manuscript was approved by all of the authors for publication.

Funding Open Access funding provided by The University of Tokyo. This study was supported in part by the New Energy and Industrial Technology Development Organization (NEDO), Japan.

Data availability No datasets were generated or analysed during the current study.

Declarations

Ethical approval and consent to participate The present study did involve any human participants or animals.

Consent for publication Not applicable.

Consent to participate Not applicable.

Competing interests The authors declare no competing interests.

Open Access This article is licensed under a Creative Commons Attribution 4.0 International License, which permits use, sharing, adaptation, distribution and reproduction in any medium or format, as long as you give appropriate credit to the original author(s) and the source, provide a link to the Creative Commons licence, and indicate if changes were made. The images or other third party material in this article are included in the article's Creative Commons licence, unless indicated otherwise in a credit line to the material. If material is not included in the article's Creative Commons licence and your intended use is not permitted by statutory regulation or exceeds the permitted use, you will need to obtain permission directly from the copyright holder. To view a copy of this licence, visit http://creativecommons.org/licenses/by/4.0/.

References

Atalla RS, Crowley MF, Himmel ME, Atalla RH (2014) Irreversible transformations of native celluloses, upon exposure to elevated temperatures. Carbohydr Polym 100:2–8. https://doi.org/10.1016/j.carbpol.2013.06.007

Bohrn R, Potthast A, Schieher S, Rosenau T, Sixta H, Kosma P (2006) The FDAM method: Determination of carboxy profiles in cellulosic materials by combining group selective fluorescence labeling with GPC. Biomacromol 7:1743–1750. https://doi.org/10.1021/bm060039h

Borrega M, Ahvenainen P, Kontturi E (2018) Impact of hydrothermal and alkaline treatments of birch kraft pulp on the levelling-off degree of polymerization (LODP) of cellulose microfibrils. Cellulose 25:6811–6818. https://doi.org/10.1007/s10570-018-2017-7

Einfeldt L, Günther W, Klemm D, Heublein B (2005) Peracetylated cellulose: end group modification and structural analysis by means of ^{1}H-NMR spectroscopy. Cellulose 12:15–24. https://doi.org/10.1007/s10570-004-5668-5

Funahashi R, Okita Y, Hondo H, Zhao M, Saito T, Isogai A (2017) Different conformations of surface cellulose molecules in native cellulose microfibrils revealed by layer-by-layer peeling. Biomacromol 18:3687–3694. https://doi.org/10.1021/acs.biomac.7b01173

Funahashi R, Ono Y, Tanaka R, Yokoi M, Daido K, Inamochi T, Saito T, Horikawa Y, Isogai A (2018) Changes in the degree of polymerization of wood celluloses during dilute acid hydrolysis and TEMPO-catalytic oxidation: Formation mechanism of disordered regions along each cellulose microfibril. Int J Biol Macromol 109:914–920. https://doi.org/10.1016/j.ijbiomac.2017.11.078

Gehmayr V, Ptthast A, Sixta H (2012) Reactivity of dissolving pulps modified by TEMPO-mediated oxidation. Cellulose 19:1125–1134. https://doi.org/10.1007/s10570-012-9729-x

Håkansson H, Ahlgren P (2005) Acid hydrolysis of some industrial pulps: effect of hydrolysis conditions and raw material. Cellulose 12:177–183. https://doi.org/10.1007/s10570-004-1038-6

Henniges U, Prohaska T, Banik G, Potthast A (2006) A fluorescence labeling approach to assess the deterioration state of aged papers. Cellulose 13:421–428. https://doi.org/10.1007/s10570-005-9030-3

Hirota M, Furihata K, Saito T, Kawada T, Isogai A (2010) Glucose/glucuronic acid alternating co-polysaccharides prepared from TEMPO-oxidized native celluloses by surface peeling. Angew Chem Int Ed 49:7670–7672. https://doi.org/10.1002/anie.201003848

Hiraoki R, Fukuzumi H, Ono Y, Saito T, Isogai A (2014) SEC-MALLS analysis of TEMPO-oxidized celluloses using methylation of carboxyl groups. Cellulose 21:167–176. https://doi.org/10.1007/s10570-013-0090-5

Hirano S, Yamagishi Y, Nakaba S, Kajita S, Funada R, Horikawa Y (2020) Artificially lignified cell wall catalyzed by peroxidase selectively localized on a network of microfibrils from cultured cells. Planta 251:104. https://doi.org/10.1007/s00425-020-03396-0

Horikawa Y, Shimizu M, Saito T, Isogai A, Imai T, Sugiyama J (2018) Influence of drying of chara cellulose on length/length distribution of microfibrils after acid hydrolysis. Int J Biolog Macromol 109:569–575. https://doi.org/10.1016/j.ijbiomac.2017.12.051

Hou G, Chitobanyong K, Takeuchi M, Shibata I, Isogai A (2023) Comprehensive study of preparation of carboxy group-containing cellulose fibers from dry-lap kraft pulps by catalytic oxidation with solid NaOCl. ACS Sustain Chem Eng 11:14782–14792. https://doi.org/10.1021/acssuschemeng.3c04750

Isogai A, Saito T, Fukuzumi H (2011) TEMPO-oxidized cellulose nanofibers. Nanoscale 3:71–85. https://doi.org/10.1039/c0nr00583e

Isogai A (2018) Development of completely dispersed cellulose nanofibers. Proc Jpn Acad Ser B 94:161–179https://doi.org/10.2183/pjab.94.012

Isogai A, Hänninen T, Fujisawa S, Saito T (2018) Review: Catalytic oxidation of cellulose with nitroxyl radicals under aqueous conditions. Prog Polym Sci 86:122–148. https://doi.org/10.1016/j.progpolymsci.2018.07.007

Jusner P, Bausch F, Schiehwer S, Schwaiger E, Potthast A, Rosenau T (2022) Protocol for characterizing the molar mass distribution and oxidized functionality profiles of aged transformer papers by gel permeation chromatography (GPC). Cellulose 29:2241–22564. https://doi.org/10.1007/s10570-022-04464-2

Kim DY, Nishiyama Y, Kuga S (2002) Surface acetylation of bacterial cellulose. Cellulose 9:361–367. https://doi.org/10.1023/A:1021140726936

Milanovic J, Schiehser S, Milanovic P, Potthast A, Kostic M (2013) Molecular weight distribution and functional group profiles of TEMPO-oxidized lyocell fibers. Carbohydr Polym 98:444–450. https://doi.org/10.1016/j.carbpol.2013.06.033

Nishiyama Y, Kim UJ, Kim DY, Katsumata KS, May RP, Langan P (2003) Periodic disorder along ramie cellulose microfibrils. Biomacromol 4:1013–1017. https://doi.org/10.1021/bm025772x

Okita Y, Saito T, Isogai A (2010) Entire surface oxidation of various cellulose microfibrils by TEMPO-mediated oxidation. Biomacromol 11:1696–1700. https://doi.org/10.1021/bm100214b

Ono Y, Isogai A (2021) Analysis of celluloses, plant holocelluloses, and wood pulps by size-exclusion chromatography/multi-angle laser-light scattering. Carbohydr Polym 251:117045. https://doi.org/10.1016/j.carbpol.2020.117045

Ono Y, Tanaka R, Funahashi R, Takeuchi M, Saito T, Isogai A (2016) SEC-MALLS analysis of ethylenediamine-pretreated native celluloses in LiCl/N, N-dimethylacetamide: softwood kraft pulp and highly crystalline bacterial, tunicate, and algal celluloses. Cellulose 23:1639–1647. https://doi.org/10.1007/s10570-016-0948-4

Ono Y, Fujisawa S, Saito T, Isogai A (2017) Branched structures of softwood celluloses: proof based on size-exclusion chromatography and multi-angle laser-light scattering. ACS Symp Seri, Am Chem Soc 1251:151–169. https://doi.org/10.1021/bk-2017-1251.ch008

Ono Y, Fujisawa S, Saito T, Isogai A (2018) Stability of branched structures of softwood cellulose, investigated by SEC/MALLS/RI/UV and sugar composition analyses. Cellulose 25:2667–2679. https://doi.org/10.1007/s10570-018-1713-7

Ono Y, Fukui S, Funahashi R, Isogai A (2019) Relationship of distribution of carboxy groups to molar mass distribution of TEMPO-oxidized algal, cotton, and wood cellulose nanofibrils. Biomacromol 20:4026–4034. https://doi.org/10.1021/acs.biomac.9b01110

Ono Y, Takeuchi M, Zhou Y, Isogai A (2021) TEMPO/NaBr/NaClO and NaBr/NaClO oxidations of cotton linters and ramie cellulose samples. Cellulose 28:6035–6049. https://doi.org/10.1007/s10570-021-03944-1

Ono Y, Takeuchi M, Isogai A (2022a) Changes in neutral sugar composition, molar mass and molar mass distribution, and solid-state structures of birch and Douglas fir by repeated sodium chlorite delignification. Cellulose 29:2119–2129. https://doi.org/10.1007/s10570-022-04448-2

Ono Y, Takeuchi M, Kimura S, Puangsin B, Wu CN, Isogai A (2022b) Structures, molar mass distributions, and morphologies of TEMPO-oxidized bacterial cellulose fibrils. Cellulose 29:4977–4992. https://doi.org/10.1007/s10570-022-04617-3

Ono Y, Hou G, Chitbanyong K, Takeuchi M, Isogai A (2023) Molar masses and molar mass distributions of commercial regenerated cellulose materials and softwood dissolving pulp determined by SEC/MALLS. Cellulose 30:8221–8233. https://doi.org/10.1007/s10570-023-05414-2

Öztürk HB, Potthast A, Rosenau T, Abu-Rous M, MacNaughtan B, Schuster KC, Mitchell JR, Bechtold T (2008) Changes in the intra- and inter-fibrillar structure of lyocell (TENCEL®) fibers caused by NaOH treatment. Cellulose 16:37–52. https://doi.org/10.1007/s10570-008-9249-x

Shinoda R, Saito T, Okita Y, Isogai A (2012) Relationship between length and degree of polymerization of TEMPO-oxidized cellulose nanofibrils. Biomacromol 13:842–849. https://doi.org/10.1021/bm2017542

Sun SJ, Imai T, Sugiyama J, Kimura S (2017) CesA protein is included in the terminal complex of Acetobacter. Cellulose 24:2017–2027. https://doi.org/10.1007/s10570-017-1237-6

Takaichi S, Saito T, Tanaka R, Isogai A (2014) Improvement of nanodispersibility of oven-dried TEMPO-oxidized celluloses in water. Cellulose 21:4093–4103. https://doi.org/10.1007/s10570-014-0444-7

Tot I, Müller Y, Werner C, Rosenau T, Potthast A (2009) A novel, mild and selective methylation of carboxyl groups in cellulosic pulps 10th EWLP, Stockholm, Sweden, August 25–28, 2008. Holzforschung 63:657–663. https://doi.org/10.1515/HF.2009.103

Yamagishi Y, Uchiyama H, Sato T, Kitamura K, Yoshimoto J, Nakaba S, Watanabe U, Funada R (2015) In vitro induction of the formation of tracheary elements from suspension-cultured cells of the conifer Cryptomeria japonica. Trees-Struct Funct 29:1283–1289. https://doi.org/10.1007/s00468-014-1139-2

Zhou Y, Saito T, Bergström L, Isogai A (2018) Acid-free preparation of cellulose nanocrystals by TEMPO oxidation and subsequent cavitation. Biomacromol 19:633–639. https://doi.org/10.1021/acs.biomac.7b01730

Zhou Y, Ono Y, Takeuchi M, Isogai A (2020) Changes to the contour length, molecular chain length, and solid-state structures of nanocellulose resulting from sonication in water. Biomacromol 21:2346–2355. https://doi.org/10.1021/acs.biomac.0c00281

Zimmermann R, Müller Y, Freudenberg U, Jehnichen D, Potthast A, Rosenau T, Werner C (2016) Oxidation and structural changes in NMMO-regenerated cellulose films. Cellulose 23:3535–3541. https://doi.org/10.1007/s10570-016-1084-x

Publisher's Note Springer Nature remains neutral with regard to jurisdictional claims in published maps and institutional affiliations.